Vertically aligned nanostructures based on Na-doped ZnO nanorods for wide band gap semiconductor memory applications

2013 Nanotechnology 24 395203

(http://iopscience.iop.org/0957-4484/24/39/395203)

IOP PUBLISHING NANOTECHNOLOGY
Nanotechnology **24** (2013) 395203 (5pp) doi:10.1088/0957-4484/24/39/395203

Vertically aligned nanostructures based on Na-doped ZnO nanorods for wide band gap semiconductor memory applications

Jian Huang, Jing Qi, Zonglin Li and Jianlin Liu

Quantum Structures Laboratory, Department of Electrical Engineering, University of California, Riverside, CA 92521, USA

E-mail: jianlin@ee.ucr.edu

Received 21 May 2013, in final form 9 August 2013
Published 6 September 2013
Online at stacks.iop.org/Nano/24/395203

Abstract
Vertically aligned undoped ZnO nanotips, nanotubes and nanorods were synthesized on the top facets of Na-doped ZnO nanorods without catalytic assistance under different growth times in a chemical vapor deposition system. The growth mechanism is discussed. The Na-doped nanorods were grown on a ZnO seed layer on Si. The p-type conductivity of the Na-doped nanorods was studied by temperature-dependent photoluminescence and nanorod back-gated field effect transistor measurements. The undoped nanorods, Na-doped nanorods and undoped seed layer form an n–p–n memory structure. The programming and retention characteristics have been demonstrated.

(Some figures may appear in colour only in the online journal)

ZnO has attracted significant attention in the past few years due to its wide band gap of 3.37 eV, large exciton binding energy of 60 meV, and easy formation of diverse nanoscale morphologies [1–4]. These various nanostructures, which can be synthesized by different methods, such as solution synthesis [5], chemical vapor deposition (CVD) [6] and physical vapor deposition (PVD) [7], have been used for various applications. For example, ZnO nanotips are an excellent structure for field emission devices [1]; ZnO tubular structures can be used as sensors due to their large surface [8]; and one-dimensional nanowires can serve as excellent optical medium for lasers [6, 9]. Although these different nanostructures (nanotips, nanotubes and nanorods) have been demonstrated separately by different methods, their controllable growth, especially in highly orientated forms, using the same technique will definitely benefit their applications and has not been reported yet. In this research, we achieved different vertically aligned one-dimensional ZnO nanostructures using CVD on top of vertically aligned Na-doped nanorods. The Na-doped nanorods were grown on a ZnO seed layer and exhibit p-type conductivity from the nanorod back-gated field effect transistor (FET) measurements. An n–p–n memory structure formed by the undoped seed layer and nanorod homojunction exhibited reasonable programming and retention characteristics.

Na-doped ZnO nanorods were grown in a quartz tube furnace system under atmospheric pressure. Zinc powder in a silica bottle was placed in the center of the quartz tube. A Si(100) substrate with a ZnO seed layer on top was kept 2 cm away from the Zn source at the downstream side. The undoped ZnO seed thin film was grown by molecular beam epitaxy. The film consists of closely packed columnar structures due to the preferential growth of wurtzite ZnO along the *c*-axis direction. The thickness of the film is about 1400 nm. The size of the substrate with the seed layer is 1 cm in width and 2 cm in length. In addition, in order to subsequently form metal contact to the undoped film, a portion of the substrate of about 0.5 cm in length was covered by a piece of silicon during the growth. $NaNO_3$ powder was placed in a silica bottle at the upstream side. Nitrogen gas with a flow rate of 1000 sccm passed continuously through the furnace as the carrier gas. The source and substrate were then heated to the growth temperature of 700 °C. During the growth, a mixture gas of argon/oxygen (99.5%/0.5%) of 300 sccm was introduced to the quartz tube. The growth time was 10 min.

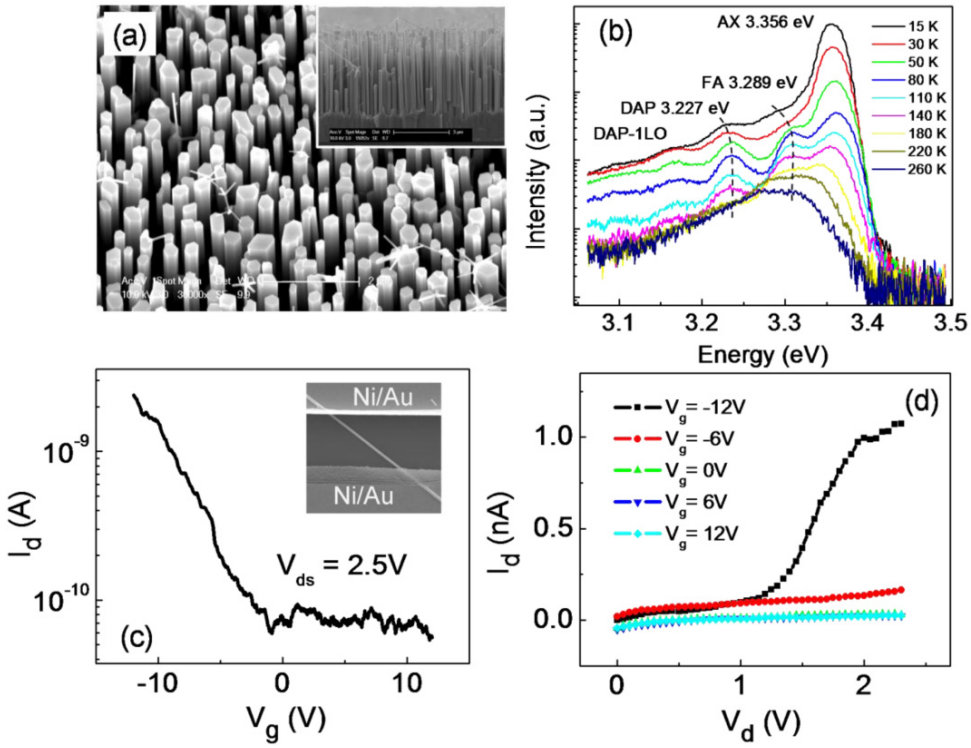

Figure 1. (a) SEM image of Na-doped ZnO nanorods. The inset is the sideview SEM image of the cleaved sample. (b) Temperature-dependent PL spectra of Na-doped ZnO nanorods. (c) I_d–V_g curve of a Na-doped nanorod back-gated FET. Inset: SEM image of the nanorod FET device. (d) I_d–V_d curves of a Na-doped ZnO nanorod back-gated FET.

Figure 1(a) shows an SEM image of the as-grown Na-doped ZnO nanorods. The inset is a side view SEM image of the cleaved sample. Na-doped vertically aligned nanorods on the ZnO seed layer are evident. The diameters of the nanorods vary and should be related to the size nonuniformity of columnar structures in the seed layer. Figure 1(b) shows the temperature-dependent photoluminescence (PL) spectra of the Na-doped ZnO nanorods. A He–Cd laser with an excitation wavelength of 325 nm was used in this experiment. The peak at 3.356 eV at 15 K can be attributed to acceptor bound exciton (AX) recombination [10–12]. The peaks at around 3.289 eV and 3.227 eV at 15 K blue-shift with increasing temperature and can be assigned to free electron to acceptor (FA) emission and donor–acceptor pair (DAP) emission, respectively [10, 13]. The longitudinal–optical (LO) phonon replica of the DAP emission at 3.157 eV is shifted by the ZnO phonon energy of ∼70 meV. The activation energy of an acceptor ΔE_A can be estimated using the equation [14] $\Delta E_A = E_{gap} - E_{DAP} - \Delta E_D + \langle \frac{e^2}{4\pi\varepsilon_0\varepsilon_{ZnO} r_{DAP}} \rangle$. The donor binding energy ΔE_D is about 30 meV [15, 16] and the intrinsic band gap $E_{gap} = 3.436$ eV at 15 K [15]. ε_{ZnO} is the dielectric constant of ZnO (8.6). r_{DAP} is the average donor–acceptor pair distance. The last term represents the Coulomb interaction between the donors and acceptors, with a value of around 20 meV [14]. Thus, the acceptor activation energy ΔE_A for the Na acceptor is estimated to be around 200 meV.

To study the electrical transport properties of the nanorods, a nanorod back-gated FET was fabricated. The Na-doped ZnO nanorods were transferred onto a SiO_2 (300 nm)/p^+-Si wafer and then Ni/Au electrodes were formed on the nanorod using photolithography and e-beam evaporation. Al was deposited on the back of the Si wafer as the back gate electrode. An SEM image of an as-fabricated device is shown in the inset of figure 1(c). The I_d–V_g curve shown in figure 1(c) exhibits the clear field effect characteristics of p-type conductivity: as the gate voltage increases, the drain current of the nanorod decreases. However, the threshold voltage is around 0 V and, therefore, the hole concentration is difficult to estimate. Considering the low drain current, this result may be due to the low hole concentration of the nanorod. The low hole concentration should be the result of strong compensation from various unintentional donors such as Zn interstitials, oxygen vacancies, and hydrogen complexes [17–19]. The low threshold voltage may also be related to the unavoidable Na contamination during the transfer of Na-doped nanorods onto the SiO_2. The mobile ion contamination is a common reason for the threshold voltage drift in a MOSFET. The output characteristics (I_d–V_d) of the device as shown in figure 1(d) also confirm the p-type conductivity. The nonlinear I_d–V_d curves indicate the existence of non-Ohmic contacts between the metal and high-resistivity p-type nanorod. However, after two months, the p-type conductivity of the nanorod decreased by about two orders of magnitude and the nanorod became highly resistive from the FET measurement. The stability of the p-type Na-doped ZnO nanorods in air is still an issue.

After the growth of Na-doped nanorods, the sample was taken out of the cooled quartz tube and immediately

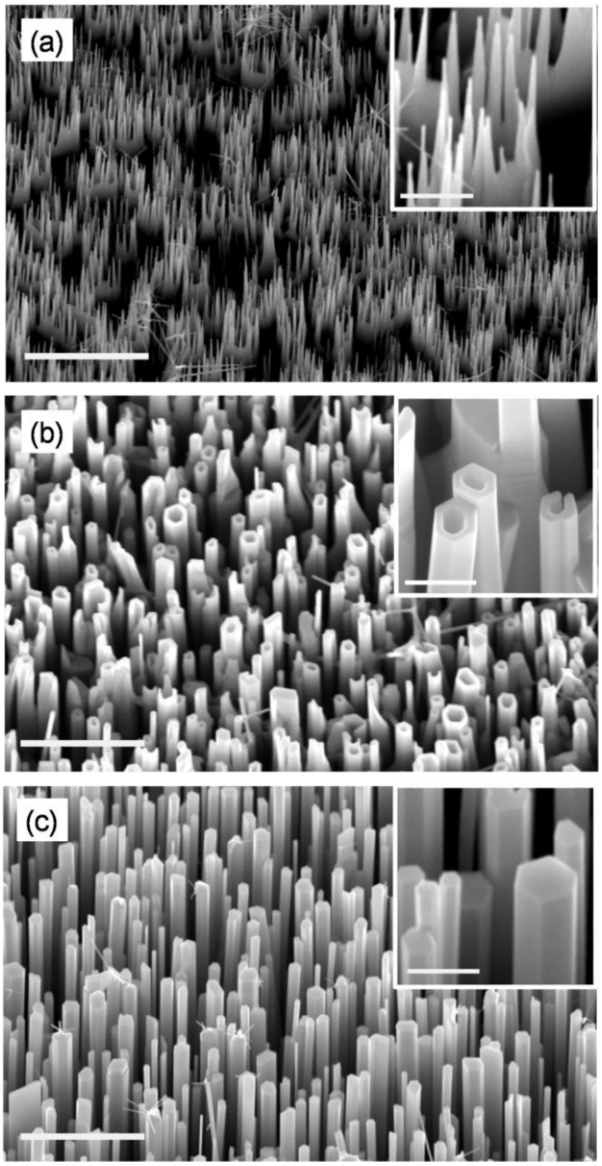

Figure 2. SEM images of different samples: (a) sample A, (b) sample B and (c) sample C. The scale bars are 3 μm. The inset of each image is the high-magnification SEM image. The scale bars are 500 nm.

transferred into another tube for subsequent growth of the undoped section. The growth configuration was the same, but without the Na source. Three samples with different growth times were grown. For sample A, the growth time of Na-doped nanorods and the undoped section on top was 4 min each. For sample B and C, the Na-doped nanorods were grown for 10 min while the undoped section growth durations were 4 min and 8 min, respectively. Different growth times lead to different types of one-dimensional ZnO nanostructures on top of these Na-doped nanorods. For sample A, after the 4 min undoped ZnO growth, vertically aligned nanotips were grown mainly at the edge of top facets of the Na-doped nanorods (figure 2(a)). Different from sample A, nanotubes were formed on top of the Na-doped nanorods in sample B (figure 2(b)) while nanorods were formed on top of the Na-doped nanorods in sample C (figure 2(c)). To investigate the growth mechanism of the nanostructures, figure 3 shows SEM images of the samples at different stages. As shown in (i)–(iii) of figure 3(a), the nucleation mainly took place at the edge of the top facets of the nanorods in sample A; as the growth time increases to 4 min, the undoped ZnO became longer, forming the nanotips. However, on the 10 min Na-doped nanorods (figure 3(b)(i)), 4 min growth of the undoped ZnO led to tubular structures (figure 3(b)(ii) and (iii)); at a longer growth time of 8 min, the tubular structures disappeared and nanorod structures formed (figure 3(b)(iv)).

Because no catalyst was used during the growth, the formation of ZnO nanostructures should follow a self-seeding vapor–solid (VS) growth mechanism. During the growth, the Zn powder was heated to form Zn vapor, which diffused out of the silica bottle and was transported by the carrier gas. At a substrate temperature of 700 °C, the desorption effect is strong and it is difficult to form ZnO seeds on the whole surface of the top facets of the short Na-doped nanorods (figure 3(a)(i)), especially under a high gas flow rate (1000 sccm N_2 and 300 sccm Ar/O_2 in the mixture), i.e., a low Zn vapor concentration. Discrete seeds formed at the edge or at some defect points on top of the nanorods (figure 3(a)(ii)). The crystals grew from the seeds and formed nanotips (figure 3(a)(iii)). In contrast, for sample B and C, the Na-doped ZnO nanorods are very dense as a result of the 10 min growth (figure 1(a) and inset); the speed of the carrier gas near the top of the nanorods was decreased. A higher Zn vapor concentration was achieved around the top of the nanorods, leading to the formation of a continuous seed layer around the edge. The ZnO walls grew from these seeds and tubular structures formed (figure 3(b)(ii)). When the tubular structure became longer, although the atom desorption was still strong due to the high temperature, the semi-enclosed tubular structures could trap the atoms, and thus a high Zn vapor concentration formed inside the nanotubes. Nucleation and growth took place inside the nanotubes. Because of the faster growth rate under the Zn-rich condition [20], the inside wall of the tubes grew faster and solid nanorods formed at a longer growth time (figure 3(b)(iii) and (iv)).

The undoped nanorod/Na-doped nanorod/undoped thin film can function as an n–p–n memory structure. Earlier efforts on n–p–n or p–n–p wide band gap memory structures were based on SiC [21] and ZnO thin films [22], and there have been no reports on nanorod structures. A demonstration of nanorod wide-bandgap semiconductor memory would represent a first step toward the ultimate scaling of this type of nonvolatile memory. Here, Ti/Au (10 nm/100 nm) was used to form Ohmic contacts on the ZnO thin film and the top end of the undoped nanorods, as shown in the inset of figure 4(a). Polymethyl methacrylate (PMMA) was spun onto the sample to protect the bottom ZnO film and the Na-doped nanorods, and to support the Ti/Au top contact to the undoped ZnO nanorod section. The top electrode is 400 μm × 400 μm. The thickness of the n-type film is about 1400 nm. The lengths of the Na-doped nanorod section and the undoped nanorod section are about 7.5 μm and 6 μm, respectively. An Agilent 81104A pulse generator was used to operate the device and the capacitance was read from an Agilent 4284A LCR meter.

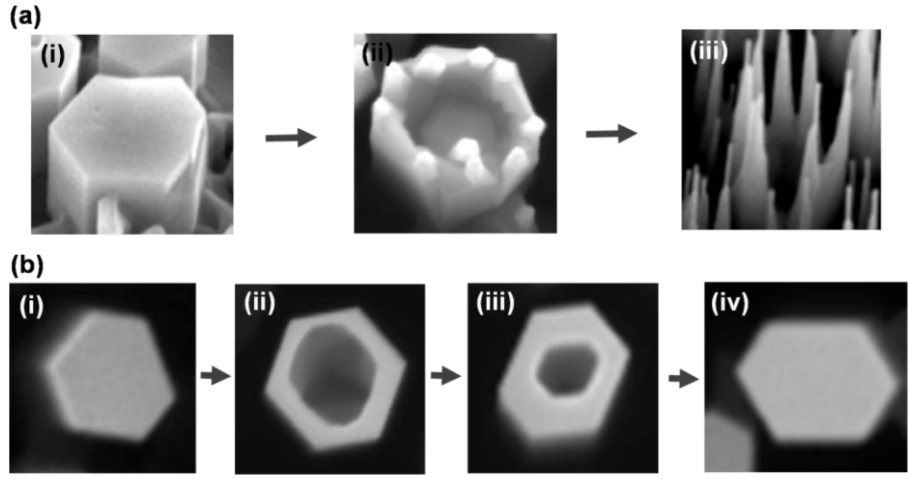

Figure 3. SEM images showing a gradual evolution process of the nanostructures. (a) Different stages of sample A from (i) the Na-doped nanorod basement, to (ii) formation of discrete ZnO seeds at the edge of the top facet, to (iii) top undoped nanotips. (b) Different stages of sample B and C from (i) Na-doped nanorod basement, to (ii) top undoped nanotube with thin wall, to (iii) top undoped nanotube with thick wall, to (iv) top undoped nanorod.

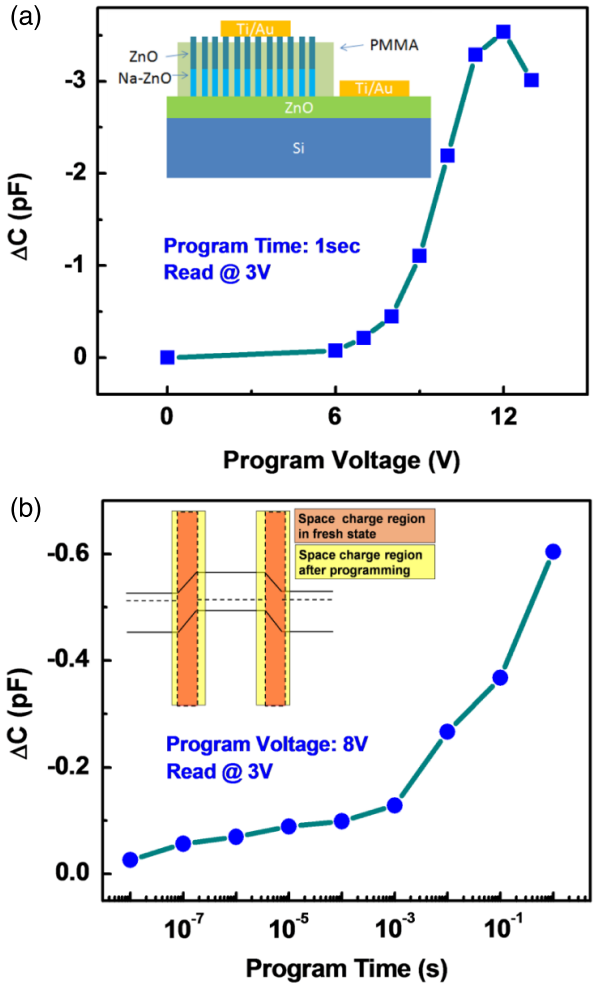

Figure 4. Programming characteristics of the ZnO n–p–n memory device. ΔC is the change of capacitance before and after programming. (a) ΔC as a function of programming pulses with different pulse heights and a 1 s pulse width. Inset: schematic of the n–p–n memory device. (b) ΔC as a function of programming pulses with different pulse widths and an 8 V pulse height. Inset: energy band diagram of the n–p–n structure, showing the space charge region before and after programming.

Figure 4(a) shows the capacitance change (ΔC) read at 3 V for different programming pulse heights. The voltage pulse width was fixed at 1 s and the pulse height was changed from 6 to 13 V. The absolute value of ΔC begins to increase once the pulse height exceeds 6 V, reaching a maximum at 12 V. Figure 4(b) shows ΔC read at 3 V as a function of different programming pulse widths. The pulse height was fixed at 8 V and the pulse width was changed from 10 ns to 1 s. The absolute value of ΔC begins to increase once the pulse width exceeds 10 ns and continues to increase as the pulse width becomes larger. The change of capacitance indicates the storage of the space charge in the memory structure. When the programming pulse is applied on the n–p–n structure, one p–n junction is forward-biased while the other one is reverse-biased. The holes inside the p-type rods flow out of the structure from the forward-biased junction and build up negative space charges inside the p-type rods. After programming, the excess space charges are stored inside the structure and reverse-bias both p–n junctions (figure 4(b) inset) leading to a decrease in the capacitance of the structure. We also note that the absolute value of ΔC decreases after a 12 V programming pulse (figure 4(a)). This should be due to the Zener effect at high voltages. The electrons at the valence band tunnel out of the p-type region through the reverse-biased junction via the forbidden gap, thus developing compensating holes in the p-type region.

After the removal of the programming voltage and at the beginning of the retention, excess space charges redistribute in the p-type section to reverse-bias both p–n junctions. Both junctions are in a nonequilibrium state and have net generation rates, thus the carriers from thermal generation will neutralize the excess space charges until both junctions return to equilibrium. This process will take an extremely long time because the thermal generation rate is exponential to the reciprocal of the band gap energy [21, 22]. Figure 5 shows the retention characteristic of the n–p–n memory structure. The capacitance decreases after the programming and increases as the waiting time increases. The extrapolation of the data

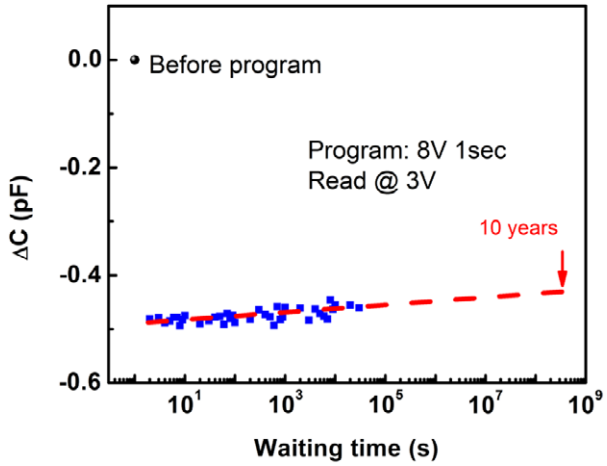

Figure 5. Retention characteristic of the ZnO n–p–n memory structure programmed at 8 V for 1 s.

suggests that there will be no significant change of capacitance even after 10 years, which indicates good retention.

In conclusion, vertically aligned Na-doped nanorods were grown on a ZnO seed layer on Si via CVD at 700 °C. The Na-doped nanorods were studied by the temperature-dependent photoluminescence and an activation energy of ∼200 meV was estimated. The p-type conductivity of the Na-doped nanorods was further confirmed by the output and transfer characteristics of the nanorod back-gated FET. Vertically aligned ZnO nanotips, nanotubes and nanorods were synthesized without catalytic assistance on the p-type Na-doped ZnO nanorods. The different morphology originates from different Zn vapor concentrations. An n–p–n memory structure based on the homojunction nanorod and undoped seed layer was fabricated. The programming and retention characteristics show a good memory effect and, in turn, confirm the formation of the p–n homojunction nanorods. These diverse vertically aligned nanostructures on p-type ZnO nanorods are promising for future nanoelectronics and optoelectronic applications.

Acknowledgments

The authors would like to thank the Department of Energy (DE-FG02-08ER46520) for p-type ZnO research and the Defense Microelectronics Activity (DMEA) under agreement number H94003-10-2-1003 for ZnO memory device work.

References

[1] Sugavaneshwar R P, Nagao T and Nanda K K 2012 *RSC Adv.* **2** 2713–6
[2] Wei Y, Ding Y, Li C, Xu S, Ryo J-H, Dupuis R, Sood A K, Polla D L and Wang Z L 2008 *J. Phys. Chem.* C **112** 18935–7
[3] She G-W, Zhang X-H, Shi W-S, Fan X, Chang J C, Lee C-S, Lee S-T and Liu C-H 2008 *Appl. Phys. Lett.* **92** 053111
[4] Yang D-S, Lao C and Zewail A H 2008 *Science* **321** 5896
[5] Xu S and Wang Z L 2011 *Nano Res.* **4** 1013–98
[6] Chu S, Wang G, Zhou W, Lin Y, Chernyak L, Zhao J, Kong J, Li L, Ren J and Liu J 2011 *Nature Nanotechnol.* **6** 506
[7] Lucas M, Wang Z L and Riedo E 2010 *Phys. Rev.* B **81** 045415
[8] Hsueh T-J, Chang S-J, Hsu C-L, Lin Y-R and Chen I-C 2008 *J. Electrochem. Soc.* **155** K152–5
[9] Huang J, Chu S, Kong J, Zhang L, Schwarz C M, Wang G, Chernyak L, Chen Z and Liu J 2013 *Adv. Opt. Mater.* **1** 179–85
[10] Liu W, Xiu F, Sun K, Xie Y-H, Wang K L, Wang Y, Zou J, Yang Z and Liu J 2010 *J. Am. Chem. Soc.* **132** 2498
[11] Liu W W, Yao B, Zhang Z Z, Li Y F, Li B H, Shan C X, Zhang J Y, Shen D Z and Fan X W 2011 *J. Appl. Phys.* **109** 093518
[12] Cao B Q, Lorenz M, Rahm A, von Wenckstern H, Czekalla C, Lenzner J, Benndorf G and Grundmann M 2007 *Nanotechnology* **18** 455707
[13] Yu D, Hu L, Qiao S, Zhang H, Len S-E A, Len L K, Fu Q, Chen X and Sun K 2009 *J. Phys. D: Appl. Phys.* **42** 055110
[14] Look D C and Claflin B 2004 *Phys. Status Solidi* b **241** 624–30
[15] Meyer B K *et al* 2004 *Phys. Status Solidi* b **241** 231–60
[16] Avrutin V, Silversmith D J and Morkoc H 2010 *Proc. IEEE* **98** 1269–80
[17] Look D C, Hemsky J W and Rizelove J R 1999 *Phys. Rev. Lett.* **82** 2552
[18] Zhang S B, Wei S H and Zunger A 2001 *Phys. Rev.* B **63** 075205
[19] Li Y J, Kaspar T C, Droubay T C, Zhu Z, Shutthanandan V, Nachimuthu P and Chambers S A 2008 *Appl. Phys. Lett.* **92** 152105
[20] Ko H-J, Yao T, Chen Y and Hong S-K 2002 *J. Appl. Phys.* **92** 4354
[21] Wang Y, Cooper J A, Melloch M R, Sheppard S T, Palmour J W and Lipkin L A 1996 *J. Electron. Mater.* **25** 899–907
[22] Huang J, Li Z L, Chu S and Liu J L 2012 *Appl. Phys. Lett.* **101** 232102